Short Communication

Disposable electrochemical sensor for the detection of lead(II) ions in the natural water

Guojing Fan[1], Xiaoyan Luo[2,]*

[1] The school of History Culture &Tourism, Ganzhou Normal University, Ganzhou, Jiangxi,341000, P.R. China
[2] The school of Business, Pingxiang University, Pingxiang, Jiangxi,337055, P.R. China
[*]E-mail: xiaoyanguo6971@163.com

The leaching of metal ions from the mines may result in pollution of the surrounding waters. In this work, we propose a composite material that combines porous carbon and graphene (G-C), which shows a very high sensitivity to lead ions. The lamellar structure of the composite material facilitates the rapid diffusion of lead ions on the surface of the material. Meanwhile, combined with the strong adsorption ability of the microporous carbon layer for heavy metal ions, the sensor has a high sensitivity towards electrochemical detection of lead ions in water. In addition, the proposed electrochemical sensor has been successfully applied for field detection.

1. INTRODUCTION

Lead is one of the metals that were first used by human, being smelted from ore and used as a building material as early as 3000 BC. The content of lead in the earth's crust is 0.0016%, making it the most abundant heavy metal, and the main ore is galena. Lead from the natural environment can be released into the atmosphere through volcanic eruptions and tsunamis. Soil is the largest reservoir of lead in the natural environment with a relatively long-lasting impact [1–6]. Lead mining has a very long history, but many of the mines are now closed. Some of these areas have been turned into tourist sites under the government's planning. However, the lead ions in the tailings will be slowly released into the environment, especially into the water environment of the landscape through rainwater [7–12].

Lead in human body mainly comes from food, breathing and drinking water, and is mostly excreted through urine and feces. However, its long biological half-life allows it to accumulate in the human body for a long time. The typical toxicological effects of lead include: affecting porphyrin

metabolism, inhibiting heme synthesis, causing hypochromic anemia, inhibiting ATP on the red blood cell membrane, causing loss of sodium and potassium ions, and resulting in hemolysis. Lead ions can damage the nervous system, inhibit myophosphate kinase, and block transmission of nerve impulses in the extensor muscles, resulting in nerve paralysis. Moreover, lead ions can also cause brain damage by breaking the blood-brain barrier and causing swelling of cells in the capillaries, leading to cerebral edema and cerebral hemorrhage [13]. Lead ions can damage the digestive system and may cause inhibition of alkaline phosphatase and ATP enzyme activity in the intestinal wall, resulting in abdominal cramps [14]. In addition, lead can directly damage liver function with spasm of small arteries in the liver, which may cause local ischemia, resulting in hepatomegaly, jaundice and even cirrhosis or liver necrosis [15].

With the frequent occurrence of lead poisoning incidents, the lead detection technology has been gradually attached much importance [16–21]. The scientific researchers around the world have been constantly seeking new breakthroughs in terms of low cost, simple operation, increased sensitivity, etc. At present, the major physicochemical methods for the detection of lead ions are atomic spectrometry, mass spectrometry, UV-visible spectrophotometry, high performance liquid chromatography and electrochemical analysis [22–28]. Electrochemical method is an analytical method established on the basis of electrochemical properties of substances in solution and at electrodes, which mainly measures electrical signal conductance, potential, current and power. This method can be recorded directly without signal conversion. Among the methods for the detection of trace heavy metal ions, electrochemical analysis has been favored by many researchers in recent years for its sensitivity, accuracy, rapidity, low cost and simplicity of operation, compared with the traditional methods with high cost and tedious operation [29–35].

Electrochemical testing techniques can be performed in the laboratory or in the field. In the case of being operated in the field, it is essential to design a disposable and rapid detection chip. Screen-printed electrodes are often adopted in the preparation of disposable electrodes for their low cost. However, carbon paste electrodes containing binder often make the sensor less effective due to their poor conductivity [36,37]. Currently, a large number of carbon nanomaterials are increasingly applied in the research of electrochemical detection of heavy metals because of their high adsorption of heavy metal ions. Porous carbon spheres are used to improve the enrichment efficiency of the electrode surface for heavy metal ions, for the reason that porous carbon spheres have a high specific surface area and abundant functional groups, which can significantly enhance the adsorption capacity of heavy metal ions, thus achieving positive detection results. In spite of so many advantages of porous carbon, its lower electron transport capacity compared with materials such as graphite dilution hinders the charge transfer between the electrode material and the surface of the glassy carbon electrode, which limits the further application of pure porous carbon in the field of electrochemical detection [38]. Graphene is a two-dimensional structured carbon material whose lamellae are formed by the interconnection of carbon atoms in a hybridized manner. Its excellent electron transport properties, the large external surface area inherent in the lamellar structure itself, and its favorable electrocatalytic properties allow it to be an ideal platform for electrode detection in the field of heavy metal detection. In addition, the single-atom thickness and two-dimensional planar structure of graphene oxide provide it with a great specific surface area, together with a structure containing a large number of boundary points, structural defects and abundant functional groups [39]. It can be compounded with other materials to synthesize a wide variety

of graphene derivatives. A number of graphene-based sensors have been designed and synthesized for heavy metal ion detection.

In this work, we designed a platform for lead ions detection in water by using the high adsorption capacity of porous carbon for heavy metal ions as well as the high electrical conductivity and lamellar structure of graphene. The graphene-porous carbon composite was successfully used for the surface modification of SPE. The formed porous carbon with microporous lamellar structure has showed good performance in strong acidic and alkaline environments, which also enhances the application value of the material.

2. MATERIALS AND METHODS

2.1. Materials

All reagents were analytical grade and used without further purification. Potassium ferricyanide ($K_4[Fe(CN)_6]\cdot 3H_2O$, potassium ferricyanide ($K_3[Fe(CN)_6]$), dipotassium hydrogen phosphate (K_2HPO_4), potassium dihydrogen phosphate (KH_2PO_4), asparaginate, standard Cd(II) and Pb(II) ions were purchased from Sinopharm Group Chemical Reagent Beijing Co., Ltd. Graphene oxide (Sheet diameter: 1-5 μm, Content: 5.0wt%, Solvent: NMP) was purchased from Nanjing XFNANO Materials Tech Co., Ltd. Conductive silver adhesive was purchased from Shanghai Baoyin Electronic Materials Co., Ltd. FR-4 glass fiber board was purchased from Xi'an Xidian Electric Material Co., Ltd. 5 mM $K_3[Fe(CN)_6]$-5 mM $K_4[Fe(CN)_6]$-0.1 M PBS (pH 7.0)-1.0 M KC1 was adopted as the impedance detection solution.

2.2. Preparation of graphene-porous carbon composite

First of all, a certain amount of asparagine was dissolved in 2 mg/mL of graphene oxide solution at 25°. After complete dissolution, resorcinol was added and stirred magnetically for 5 min. Subsequently, 5 mL formic acid (37 wt%) was quickly added to the solution. After being well-stirred, the reaction was sealed and transferred to 90° for 18 h. The obtained polymer dispersion was charred at 800° under inert atmosphere to obtain the sample. By varying the mass ratio of carbon precursor to GO (5:1, 10:1, 20:1 and 40:1), a series of composites (denoted as G-C-1, G-C-2, G-C-3 and G-C-4) were obtained. The composites were then dispersed in NMP to form 2 mg/mL slurry.

2.3. Integrated G-C electrode fabrication:

An appropriate amount of G-C slurry was added to the Petri dish, and was well-scraped with a scraper to obtain a uniform sticky conductive paste. The polyethylene self-adhesive presenter board was pasted onto a cleanly treated FR-4 glass fiberboard substrate (the fiberboard was washed with ethanol and distilled water, and dried at room temperature). An integrated three-electrode system containing a G-C working electrode, a carbon counter electrode and a carbon reference electrode was obtained by

screen printing technique. Afterwards, 1 layer of silver paste was evenly coated at the reference electrode and the prepared integrated electrode was dried in an oven at 70°C. An appropriate amount of 0.1 M $FeCl_3$ solution was dropped on the silver surface, and the silver was oxidized to $FeCl_3$. After 1 h, the $FeCl_3$ solution was removed by rinsing with distilled water and air-dried to obtain the Ag/AgCl reference electrode. Finally, all areas except the working electrode, counter electrode, reference electrode and wire connection points were insulated with insulating tape.

3. RESULTS AND DISCUSSION

The scanning electron microscope visualizes the morphological structure of the synthesized composites. As shown in Figure 1, the composites have a regular lamellar structure similar to that of graphene. It is apparent that the macromolecule acts as a structural guide during the surface self-assembly process. It can be noted from the figure that the size of the lamellar structural units varies from a few tens of nanometers to more than ten microns in size. These lamellar units of different sizes lap each other, forming abundant macroporous voids that significantly increase the exposed external specific surface area of the sample. Interconnected carbon framework would effectively improve the electronic conductivity and mechanical integrity of the electrode [40]. This feature would be beneficial to the increase of the diffusion rate of heavy metal ions inside the material. In addition, the lamellar units of this series of composites have increasing thicknesses and highly flat surfaces, with average lamellar thicknesses measured at 11.4 nm, 20.2 nm, 33.7 nm and 71.5 nm. The morphology of the sample can be controlled.
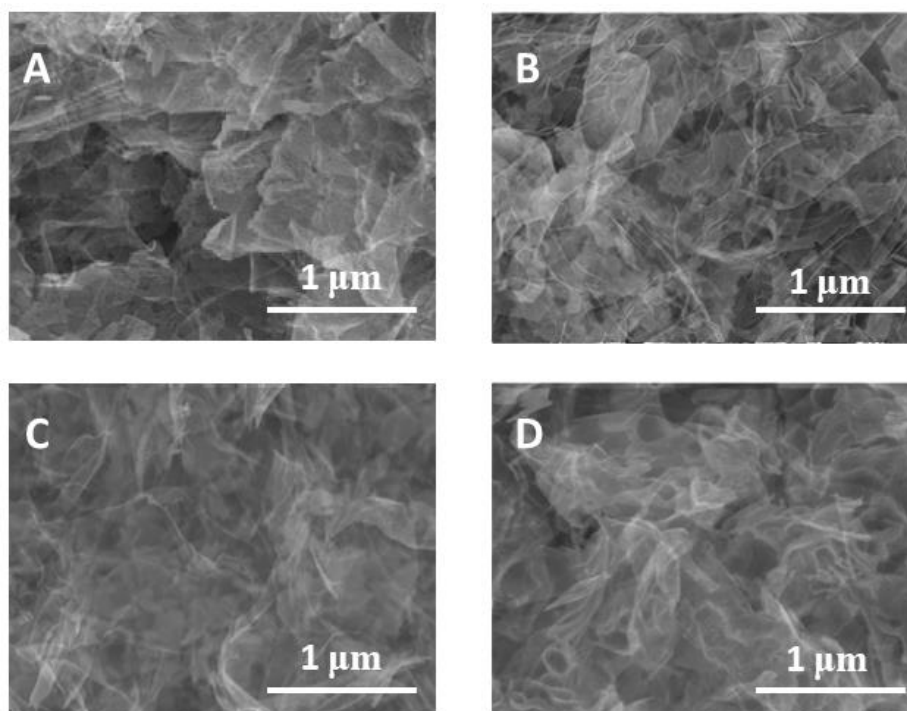

Figure 1. SEM images of (A) G-C-1, (B) G-C-2, (C) G-C-3 and (D) G-C-4.

To further observe the microstructure of the sample, XRD was adopted to characterize the crystal structure of the sample at different stages of the reaction process. Figure 2A shows a sharp peak at 10.5° in the graphite oxide, corresponding to the 001 crystal plane of graphite oxide. After 18 h of reaction at 90°, the GO-formic acid only has a peak present at 19.7° and does not show the characteristic peak of GO, indicating that the monolayer of graphite oxide is symmetrically encapsulated by the polymer layers on both sides, which in turn leads to the horizontal dispersion of the monolayer of graphite oxide [41]. After pyrolysis, it was reduced in situ to graphitic oxide while the surface was coated with a microporous carbon layer. The characteristic peak of graphitic refining does not appear in the sample after pyrolysis. Only a broad peak at 10°-30° appears, indicating the characteristic amorphous carbon structure of the sample. Since the graphite refining in the middle of the interlayer has excellent electron transport ability, it can be inferred that the composite will exhibit better electrochemical properties compared to the pure microporous carbon.

The thickness and surface area of the samples were also measured, as shown in Figure 2B. Detailed studies on the porosity characteristics were analyzed with N_2 adsorption–desorption measurements, obtained at 77 K up to a maximum relative pressure of 1 bar. G-C-4 had the thickest lamellae among all samples, while G-C-1 had the thinnest.
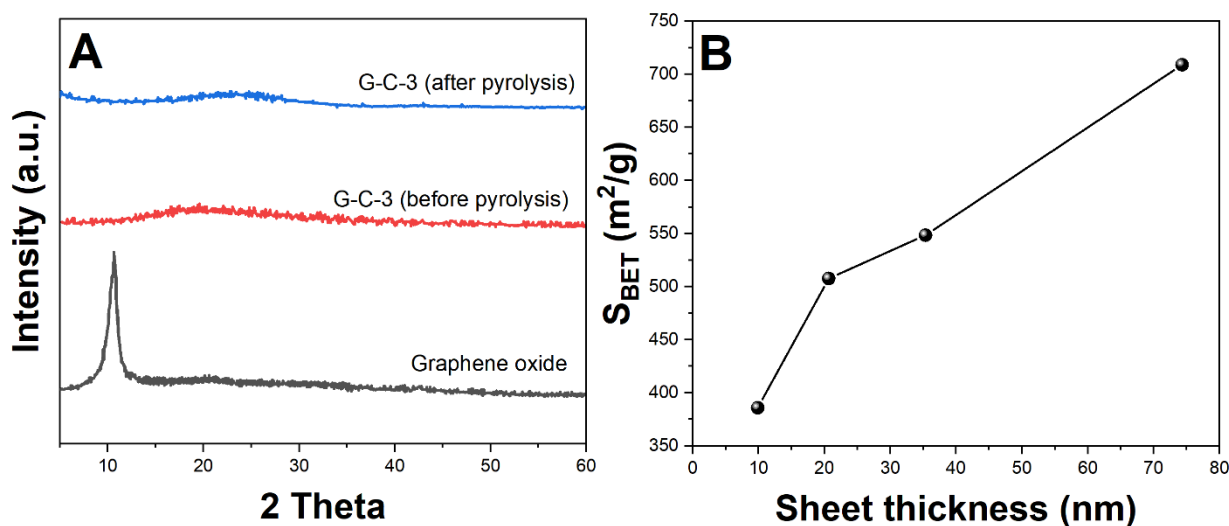

Figure 2. (A) XRD patterns of GO, G-C-3 before and after the pyrolysis. (B) The relationship between the thickness of sheets and the surface area of G-C samples.

To explore where the pattern of the samples came from, we made a fitted curve of the increase and decrease relationship of this variable with the ratio table and lamellar thickness data of these four samples, which can for instance be caused by the existence of non-rigid aggregates of single to a few-layered graphene structures or assemblages of slit-shaped mesopores [42]. It can be clearly seen from the figure that the specific surface area increases with the lamella thickness. The trend of its specific surface area increase is consistent with the order of lamella thickness. Especially in the initial stage, the enhancement of specific surface area slows down with the thickening of the lamellar structure unit, the

reason for which is that the specific surface area is mainly from the microporous carbon layer wrapped around the graphite thin flakes. The amount of graphene oxide is fixed during the synthesis process, and a high ratio of carbon precursor to graphene oxide mass leads to a result that the thicker the flake layer is, the higher the specific surface area will be. Considering the large specific surface area and suitable pore size provided by the microporous carbon layer, its strong adsorption ability on heavy metal ions will contribute to the detection effect.

We used anodic stripping square wave voltammetry (SWSVA) for the screen-printed electrodes prepared with different G-C composite for electrochemical detection of lead ions in water. Figure 3 shows the response signals of the chip prepared from G-C-1, G-C-2, G-C-3 and G-C-4 composites toward different concentrations of lead solutions in water. A very sharp peak appeared at -0.6 V corresponding to the dissolution of lead ions [43]. Meanwhile, the current values obtained by electrochemical tests for all four chips were fitted and a linear relationship was formed.
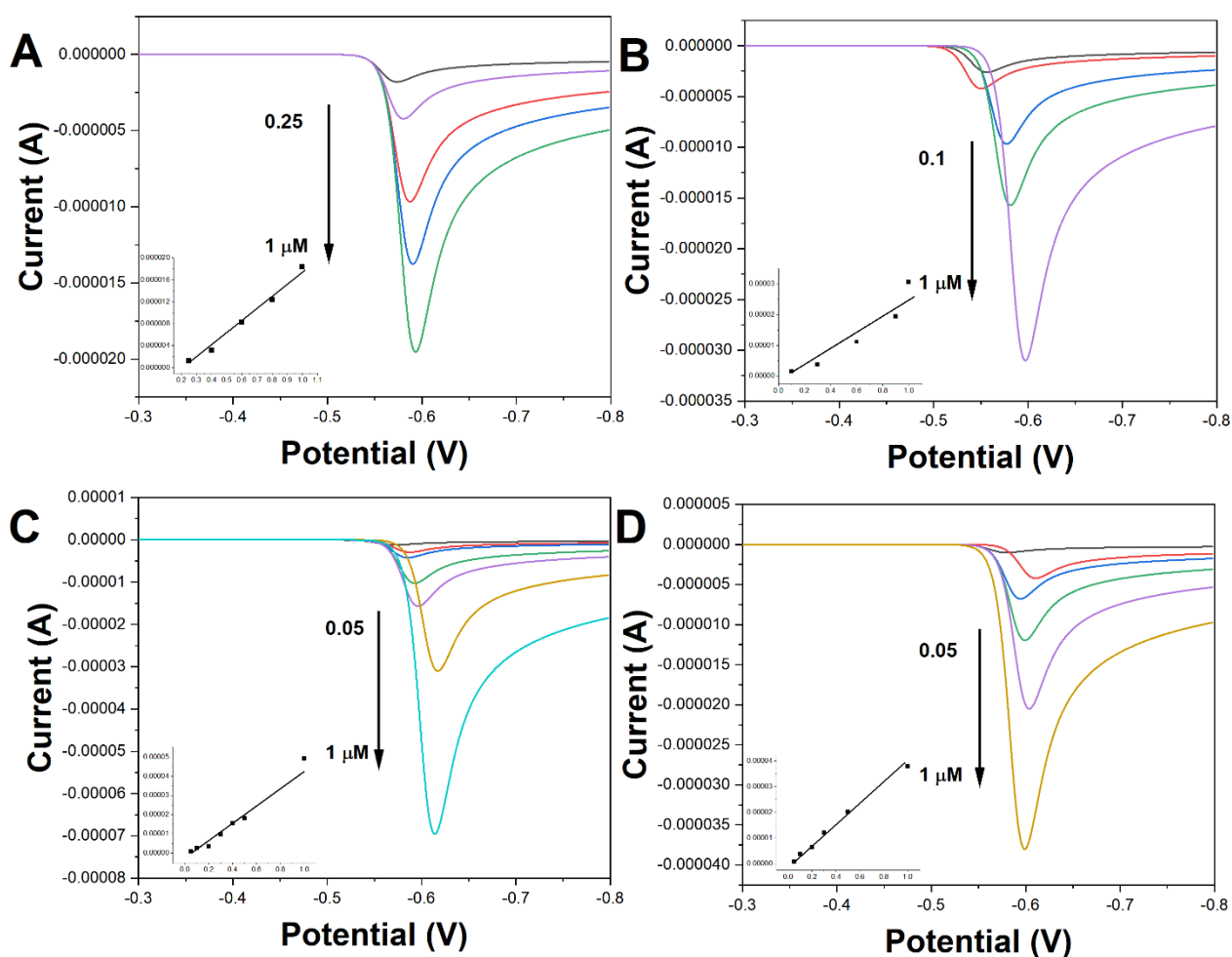

Figure 3. SWASV of (A) G-C-1/SPE, (B) G-C-2/SPE, (C) G-C-3/SPE and (D) G-C-4/SPE towards different concentrations of lead ions in 0.1 M NaAc-Hac (pH=5). Inset: plots of lead ions concentrations against peak current.

It is well known that the efficiency of lead ion pre-accumulation on the electrode surface is significant for the effectiveness of electrochemical detection. The ability to obtain high sensitivity and low detection limits during the detection process is partly determined by the strong adsorption capacity of the microporous carbon layer for the target ions [44–46]. In this part of the work, the positive detection performance is partly resulted from the high specific surface area of the sample, which provides more active sites during lead ion adsorption. In addition, the adsorption rate of the material is equally important in fast electrochemical detection. The graded pore structure of the material and the large external surface area of the lamellar structure itself enable the lead ions in solution to contact the material surface more easily and achieve a higher adsorption rate.

The electrical conductivity of both G-C/SPE is high, which is mainly due to the role of graphitic flakes in the composite. Graphite dilution as a conductive medium significantly facilitates the charge transfer process within the material. The higher the relative amount of added graphene is and the thinner the flake layer is, the higher the conductivity will be. As shown in Table 1, the material conductivity shows a high regularity with respect to the flake layer thickness.

Both G-C/SPE have shown a high sensitivity for lead ion detection. Among the four sensors, their detection sensitivity increases in the order of G-C-4/SPE < G-C-1/SPE < G-C-2/SPE < G-C-3/SPE. Although G-C-4 has the thickest flake layer, it has the lowest sensitivity.

Table 1. Electrochemical performance of the G-C/SPE with other reports toward lead ions detection.

Sensor	Conductivity (S/cm)	Linear detection range (µM)	Limit of detection (µM)	Reference
Bi/MGF–Nafion/GCE	-	0.08-3.12 µM	0.02 µM	[47]
Bi/Nafion/RGO-GNPs/GCE	-	0.2-0.9 µM	0.14 µM	[48]
Diatomite–MPTMS/GCE	-	2-15 µM	1.23 µM	[49]
PyTS–CNTs/Nafion/PGE	-	0.1-3 µM	0.05 µM	[50]
G-C-1/SPE	18.9	0.25-1 µM	0.08 µM	This work
G-C-2/SPE	9.0	0.1-1 µM	0.04 µM	This work
G-C-3/SPE	1.1	0.05-1 µM	0.01 µM	This work
G-C-4/SPE	0.7	0.05-1 µM	0.03 µM	This work

After the detection of individual ions, the best G-C-3/SPE was adopted to detect mixed ions of lead and cadmium. Figure 4 presents that in the mixed state, cadmium ion and lead ion showed separate dissolution peaks at -0.81 V and -0.56 V, respectively. The potential interval between each dissolution peak is large enough not to interfere with each other. Therefore, the selective detection of lead ions by G-C-3/SPE is highly positive, which improves its practical application.
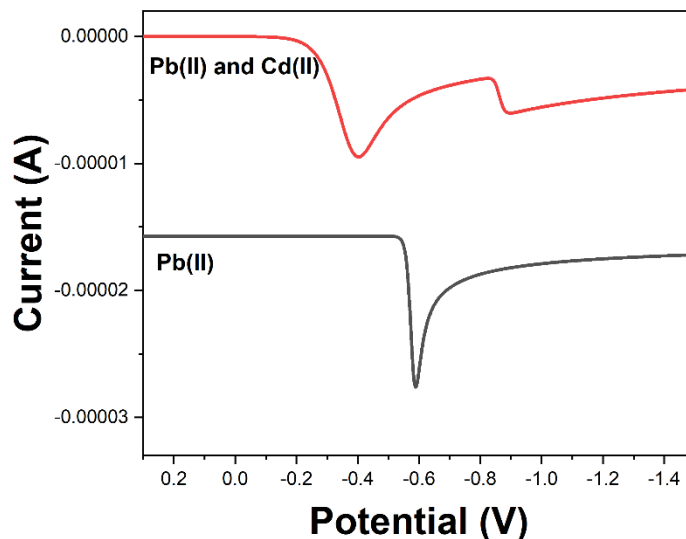
Int. J. Electrochem. Sci., 16 (**2021**) Article ID: 210924

8

Figure 4. SWASV of G-C-3/SPE for the analysis of Cd(II) and Pb(II) in 0.1 M NaAc-Hac (pH=5)..

Water samples from three scenic spots were tested with G-C-3/SPE. All three scenic areas have lead mining around them. Table 2 shows the detection results, which indicates that the presence of trace amounts of lead ions can be detected in site 3. Standard addition was also used for the measurement and the recovery rate can be calculated to be 95.0% to 105.0%.

Location	Detection	Addition	Detection	Recovery
Site 1	-	2.0 μM	2.1 μM	105.0%
Site 2	-	2.0 μM	1.9 μM	95.0%
Site 3	0.7 μM	2.0 μM	2.6 μM	96.3%

4. CONCLUSION

In this paper, a G-C composite obtained from incorporation of graphene oxide with porous carbon is reported, and it is applied to the electrochemical detection of lead ions in water, achieving a highly positive detection results. The SPE made of G-C composite has excellent performance in the detection of trace lead ions in water, and the individual values are far below the safe concentration of lead ions in drinking water set by the World Health Organization. The excellent detection performance of the sensor can be attributed to the porous structure of the microporous carbon layer and the good electrical conductivity of graphene. In addition, the proposed electrochemical sensor has been successfully applied in field testing.

References

1. M. Baghayeri, A. Amiri, B. Maleki, Z. Alizadeh, O. Reiser, *Sens. Actuators B Chem.*, 273 (2018)

1442–1450.

2. B. Bansod, T. Kumar, R. Thakur, S. Rana, I. Singh, *Biosens. Bioelectron.*, 94 (2017) 443–455.

3. Z. Danyıldız, D. Uzun, T.T. Calam, E. Hasdemir, *J. Electroanal. Chem.*, 805 (2017) 177–183.

4. B. Fan, Q. Wang, W. Wu, Q. Zhou, D. Li, Z. Xu, L. Fu, J. Zhu, H. Karimi-Maleh, C.-T. Lin, *Biosensors*, 11 (2021).

5. L. Fu, Z. Liu, J. Ge, M. Guo, H. Zhang, F. Chen, W. Su, A. Yu, *J. Electroanal. Chem.*, 841 (2019) 142–147.

6. H. Karimi-Maleh, M. Alizadeh, Y. Orooji, F. Karimi, M. Baghayeri, J. Rouhi, S. Tajik, H. Beitollahi, S. Agarwal, V.K. Gupta, S. Rajendran, S. Rostamnia, L. Fu, F. Saberi-Movahed, S. Malekmohammadi, *Ind. Eng. Chem. Res.*, 60 (2021) 816–823.

7. M.A. Deshmukh, R. Celiesiute, A. Ramanaviciene, M.D. Shirsat, A. Ramanavicius, *Electrochimica Acta*, 259 (2018) 930–938.

8. M.A. Deshmukh, M. Gicevicius, A. Ramanaviciene, M.D. Shirsat, R. Viter, A. Ramanavicius, *Sens. Actuators B Chem.*, 248 (2017) 527–535.

9. Y. Hu, M. Wu, R. Liu, W. Sun, *Miner. Eng.*, 150 (2020) 106272.

10. L. Fu, W. Su, F. Chen, S. Zhao, H. Zhang, H. Karimi-Maleh, A. Yu, J. Yu, C.-T. Lin, *Bioelectrochemistry* (2021) 107829.

11. G. Liu, X. Yang, H. Zhang, L. Fu, *Int J Electrochem Sci*, 15 (2020) 5395–5403.

12. H. Karimi-Maleh, A. Ayati, R. Davoodi, B. Tanhaei, F. Karimi, S. Malekmohammadi, Y. Orooji, L. Fu, M. Sillanpää, *J. Clean. Prod.*, 291 (2021) 125880.

13. J.-Y. Huang, L. Zhao, W. Lei, W. Wen, Y.-J. Wang, T. Bao, H.-Y. Xiong, X.-H. Zhang, S.-F. Wang, *Biosens. Bioelectron.*, 99 (2018) 28–33.

14. H. Konishi, T. Minato, T. Abe, Z. Ogumi, *Mater. Chem. Phys.*, 226 (2019) 1–5.

15. L. Li, D. Liu, A. Shi, T. You, *Sens. Actuators B Chem.*, 255 (2018) 1762–1770.

16. B. Molinero-Abad, D. Izquierdo, L. Pérez, I. Escudero, M.J. Arcos-Martínez, *Talanta*, 182 (2018) 549–557.

17. A.K. NS, A. S, P. Malingappa, *J. Environ. Chem. Eng.*, 6 (2018) 6939–6946.

18. L. Fu, A. Wang, G. Lai, W. Su, F. Malherbe, J. Yu, C.-T. Lin, A. Yu, *Talanta*, 180 (2018) 248–253.

19. W. Long, Y. Xie, H. Shi, J. Ying, J. Yang, Y. Huang, H. Zhang, L. Fu, *Fuller. Nanotub. Carbon Nanostructures*, 26 (2018) 856–862.

20. W. Wu, M. Wu, J. Zhou, Y. Xu, Z. Li, Y. Yao, L. Fu, *Sens. Mater.*, 32 (2020) 2941–2948.

21. Y. Xu, Y. Lu, P. Zhang, Y. Wang, Y. Zheng, L. Fu, H. Zhang, C.-T. Lin, A. Yu, *Bioelectrochemistry*, 133 (2020) 107455.

22. F.E. Salih, A. Ouarzane, M. El Rhazi, *Arab. J. Chem.*, 10 (2017) 596–603.

23. A. Waheed, M. Mansha, N. Ullah, *TrAC Trends Anal. Chem.*, 105 (2018) 37–51.

24. L. Fu, Q. Wang, M. Zhang, Y. Zheng, M. Wu, Z. Lan, J. Pu, H. Zhang, F. Chen, W. Su, *Front. Chem.*, 8 (2020) 92.

25. J. Zhou, Y. Zheng, J. Zhang, H. Karimi-Maleh, Y. Xu, Q. Zhou, L. Fu, W. Wu, *Anal. Lett.*, 53 (2020) 2517–2528.

26. M. Zhang, B. Pan, Y. Wang, X. Du, L. Fu, Y. Zheng, F. Chen, W. Wu, Q. Zhou, S. Ding, *ChemistrySelect*, 5 (2020) 5035–5040.

27. H. Karimi-Maleh, F. Karimi, M. Alizadeh, A.L. Sanati, *Chem. Rec.*, 20 (2020) 682–692.

28. H. Karimi-Maleh, F. Karimi, S. Malekmohammadi, N. Zakariae, R. Esmaeili, S. Rostamnia, M.L. Yola, N. Atar, S. Movaghgharnezhad, S. Rajendran, A. Razmjou, Y. Orooji, S. Agarwal, V.K. Gupta, *J. Mol. Liq.*, 310 (2020) 113185.

29. W. Wang, N. Bao, W. Yuan, N. Si, H. Bai, H. Li, Q. Zhang, *Microchem. J.*, 148 (2019) 240–247.

30. Y. Yao, H. Wu, J. Ping, *Food Chem.*, 274 (2019) 8–15.

31. X. Zhang, R. Yang, Z. Li, M. Zhang, Q. Wang, Y. Xu, L. Fu, J. Du, Y. Zheng, J. Zhu, *Rev. Mex. Ing. Quím.*, 19 (2020) 281–291.

32. R. Yang, B. Fan, S. Wang, L. Li, Y. Li, S. Li, Y. Zheng, L. Fu, C.-T. Lin, *Micromachines*, 11 (2020)

967.

33. L. Fu, Y. Zheng, P. Zhang, J. Zhu, H. Zhang, L. Zhang, W. Su, *Electrochem. Commun.*, 92 (2018) 39–42.

34. H. Karimi-Maleh, Y. Orooji, A. Ayati, S. Qanbari, B. Tanhaei, F. Karimi, M. Alizadeh, J. Rouhi, L. Fu, M. Sillanpää, *J. Mol. Liq.* (2020) 115062.

35. H. Karimi-Maleh, Y. Orooji, F. Karimi, M. Alizadeh, M. Baghayeri, J. Rouhi, S. Tajik, H. Beitollahi, S. Agarwal, V.K. Gupta, *Biosens. Bioelectron.* (2021) 113252.

36. L. Fu, Y. Zheng, P. Zhang, H. Zhang, Y. Xu, J. Zhou, H. Zhang, H. Karimi-Maleh, G. Lai, S. Zhao, W. Su, J. Yu, C.-T. Lin, *Biosens. Bioelectron.*, 159 (2020) 112212.

37. A.U. Alam, M.M.R. Howlader, N.-X. Hu, M.J. Deen, *Sens. Actuators B Chem.*, 296 (2019) 126632.

38. G. Ran, F. Wu, X. Ni, X. Li, X. Li, D. Liu, J. Sun, C. Xie, D. Yao, W. Bai, *Sens. Actuators B Chem.*, 320 (2020) 128326.

39. J. Wang, W. Zhu, T. Zhang, L. Zhang, T. Du, W. Zhang, D. Zhang, J. Sun, T. Yue, Y.-C. Wang, J. Wang, *Anal. Chim. Acta*, 1100 (2020) 57–65.

40. J. Wu, X. Qin, H. Zhang, Y.-B. He, B. Li, L. Ke, W. Lv, H. Du, Q.-H. Yang, F. Kang, *Carbon*, 84 (2015) 434–443.

41. G. Sun, B. Li, J. Ran, X. Shen, H. Tong, *Electrochimica Acta*, 171 (2015) 13–22.

42. A. Ganesan, M.M. Shaijumon, *Microporous Mesoporous Mater.*, 220 (2016) 21–27.

43. L. Yu, P. Zhang, H. Dai, L. Chen, H. Ma, M. Lin, D. Shen, *RSC Adv.*, 7 (2017) 39611–39616.

44. J.-Y. Hu, Z. Li, C.-Y. Zhai, J.-F. Wang, L.-X. Zeng, M.-S. Zhu, *Rare Met.*, 40 (2021) 1727–1737.

45. B. Patella, R. Russo, A. O'Riordan, G. Aiello, C. Sunseri, R. Inguanta, *Talanta*, 221 (2021) 121643.

46. Z. Wang, Y. Qin, C. Wang, L. Sun, X. Lu, X. Lu, *Appl. Surf. Sci.*, 258 (2012) 2017–2021.

47. L. Xiao, B. Wang, L. Ji, F. Wang, Q. Yuan, G. Hu, A. Dong, W. Gan, *Electrochimica Acta*, 222 (2016) 1371–1377.

48. G. Zhao, H. Wang, G. Liu, Z. Wang, J. Cheng, *Ionics*, 23 (2017) 767–777.

49. D. Quang Khieu, B.H. Dang Son, V. Thi Thanh Chau, P. Dinh Du, N. Hai Phong, N. Thi Diem Chau, *J. Chem.*, 2017 (2017) 9560293.

50. R. Jiang, N. Liu, S. Gao, X. Mamat, Y. Su, T. Wagberg, Y. Li, X. Hu, G. Hu, *Sensors*, 18 (2018) 1567.